Numerical Analysis of the Two-material Downhole Flow Field in Hydrothermal Jet Drilling

Zehao Lyu, Xianzhi Song, Gensheng Li, Zhongwei Huang, Haizhu Wang, Xiaodong Hu, Yu Shi

State Key Laboratory of Petroleum Resources and Prospecting, China University of Petroleum, Beijing, Beijing 102249, China

Keywords

hydrothermal jet; two material; cooling configuration; downhole flow field; numerical simulation

ABSTRACT

The downhole flow field of the lateral cooling configuration in hydrothermal jet drilling is investigated and compressible fluid with both water and carbon dioxide is considered. Distributions of fluid properties are analyzed. Influences of the jet velocity, jet temperature, cooling water velocity, and carbon dioxide volume fraction on the flow field are discussed. Results indicate that the simulation results in this paper are reasonable for engineering calculations. The increase of jet velocity has no obvious effect on the overall distributions of water and carbon dioxide. However, the velocity of the hydrothermal jet needs to be controlled well during drilling in the field. As the increase of jet velocity, the bottomhole pressure becomes higher. The jet temperature may reduce the jet pressure. The cooling water velocity can lower the annular temperature, but the effect on the pressure has to be further studied. The increase of water fraction may raise the jet pressure slightly.

1. Introduction

Hydrothermal jet drilling is a technology, which has the potential to be applied in the drilling for geothermal energy in deep hard formations [1, 2]. Besides the high temperature effect [3, 4], we intend to consider the effect of high pressure impact [5, 6].

This technique is a contact-free technology with coiled tubing used for continuous penetration. It can reduce the abrasion and tripping time. Fuel, oxidizer and cooling water are injected through respective channels in the coiled tubing to the downhole combustion chamber. The chemical reaction between the fuel and the oxidizer in the chamber is initiated by an electric spark. Thus, the reaction products, which are water and carbon dioxide, are discharged from the nozzle in the bottomhole assembly to impinge the rock. Meanwhile, cooling water flows out from the lateral outlet of coiled tubing and returns to the surface through the annulus. This can cool the wellbore

and coiled tubing simultaneously, and avoid the thermal destruction on the borehole wall by the high temperature fluids. Moreover, the circulation of cooling water can increase the cuttings transport efficiency. Thermal insulation is applied around coiled tubing to prevent the cooling water from influences of reservoir temperature or combustion.

In 2016, Song et al. investigated the downhole flow field and the thermo-physical interaction between wellbore fluid and ambient rock of multi-orifice nozzle hydrothermal jet [1]. Besides, Song et al. proposed and compared two kinds of cooling configurations (Lateral configuration and downward configuration) for a single hydrothermal jet drilling [2]. Incompressible fluid was assumed and only water is considered in the flow field.

In this paper, compressible fluid with both water and carbon dioxide is considered and the downhole flow field of the lateral cooling configuration is investigated. **Fig. 1** illustrates the details of the cooling configuration where the red region represents thermal fluid and blue region represents cooling water. Distributions of downhole thermal-physical properties are analyzed to indicate the accuracy of the simulation results. Influences of the jet velocity, jet temperature, cooling water velocity, and carbon dioxide volume fraction on the flow field are discussed.

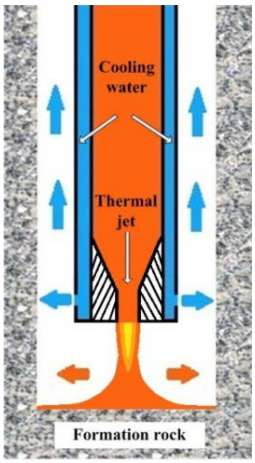

Figure 1: Lateral cooling configuration

2. Model Setup

2.1 Physical model

To simplify the numerical simulation of this axisymmetric circular drilling model, a two-dimensional model is used to represent the real three-dimensional situation as shown in **Fig. 2**. According to the cooling configurations described above, the hydrothermal jet, including water and carbon dioxide, is discharged from the central nozzle, while the cooling water flows out from the lateral outlets. To ensure the results could reflect the distribution regularities of the hydrothermal jet in the entire wellbore, the length of the wellbore is set as 300 mm. The borehole diameter is set as 50.8 mm. The coiled tubing diameter is 25.4 mm. The jet nozzle diameter and the cooling water inlet are 10 mm. Mesh is generated by Gambit using structural grids. Because the analyzed region is very short compared to the thousands of meters of well depth, friction loss between the fluid and wellbore is neglected. **Fig. 2** shows the mesh when the standoff distance is 30 mm and mesh interval size is 1.

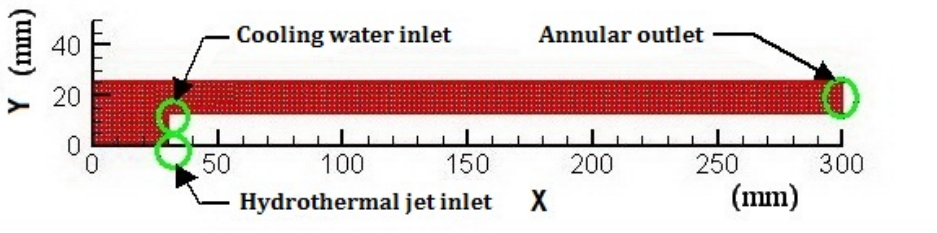

Figure 2: Mesh of the model of standoff distance 30mm

Recognizing the process of hydrothermal jet drilling, the boundary conditions are set as follows: velocity inlet boundary conditions are set for the hydrothermal jet and cooling water inlets. Outflow boundary condition: all the injected fluid flows out from the annulus. Stationary wall boundary condition: in the process of numerical simulation, the wellbore and the drilling pipe are stationary. Besides, the operating pressure is set as 30 MPa to model the environment at the depth approximately 3000 m in the reservoir.

2.2 Thermo-physical properties of supercritical water

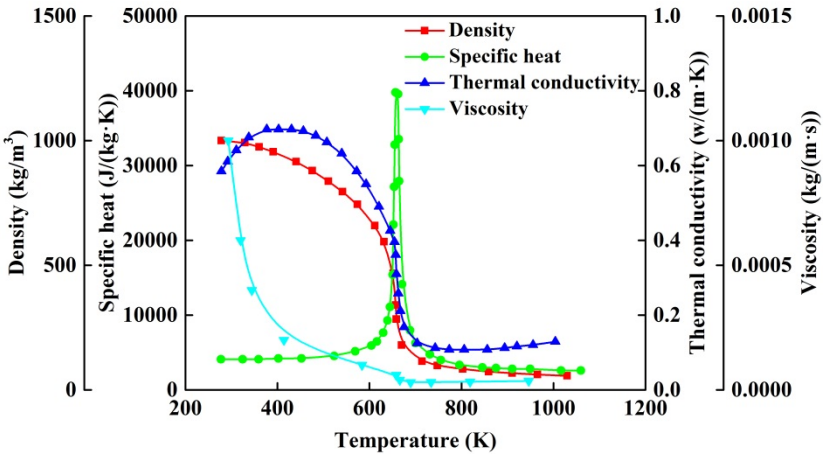

Figure 3: Thermo-physical properties of water at the pressure of 30 MPa

When the high-temperature hydrothermal jet encounters with the peripheral cooling water, drastic heat and momentum transfer occur. The simulation of supercritical water with varying thermo-physical properties is rather complicated [7, 8]. Four characteristics of water, including density, specific heat capacity, viscosity and thermal conductivity, are the most important factors in the calculation of the jet process. In this paper, the varying trends of water density and specific heat capacity are shown in **Fig. 3** at the pressure of 30 MPa [9, 10].

The water density decreases as the rise of temperature, which can be as low as 100 kg/m^3. However, the specific heat capacity changes in a wide range. For each supercritical pressure, there is a corresponding temperature yielding the maximum value of specific heat capacity at the so-called pseudo-critical point (PCP). This temperature is called the pseudo-critical temperature (PCT). The line connecting all these pseudo-critical points is named pseudo-critical line (PCL). In the vicinity of this PCL, all thermo-physical properties are very sensitive to temperature variations by undergoing sharp changes. In **Fig. 3**, the specific heat capacity changes sharply at the temperature about 675 K. In order to simulate the process of water thermo-physical property

change more accurately, the least square method with piecewise-polynomial equations is adopted to simulate the varying of water property change.

2.3 Equation of state

The Peng-Robinson equation of state is applied in the simulation of property change for carbon dioxide. Peng-Robinson is a model that is commonly used both in industry and academia as it is relatively accurate for the prediction of vapor pressure, density and other thermo-dynamic properties of non-polar and slightly polar fluids [11]. Because the molecule of carbon dioxide tends to be non-polar, the Peng-Robinson equation of state may be sufficient for the modeling.

The general form of pressure P for the cubic equation of state model is written as:

$$P = \frac{RT}{V - b + c} - \frac{\alpha}{(V^2 + \delta V + \varepsilon)} \tag{1}$$

Where P represents the absolute pressure, Pa. V represents the specific molar volume, m^3/kmol. T is the temperature, K. R is the universal gas constant. In addition, the coefficients α, b, c, δ and ε are given for each equation of state as functions of the critical temperature T_c, critical pressure P_c, acentric factor ω and critical volume V_c. The attractive coefficient α also has a temperature dependence.

$$\alpha(T) = \alpha_0[1 + n(1 - (T / T_c)^{0.5}]^2 \tag{2}$$

$$\alpha_0 = \frac{0.457247 R^2 T_c^2}{P_c} \tag{3}$$

$$b = \frac{0.07780 R T_c}{P_c} \tag{4}$$

$$n = 0.37464 + 1.54226\omega - 0.26992\omega^2 \tag{5}$$

Besides, δ is set equal to $2b$. ε is equal to $-b^2$ and c is set to zero.

2.4 Modeling method

To keep the water jet in critical state, the temperature is initially set as 673 K. The hydrothermal jet velocity is set as 100 m/s according to the general velocity of the high pressure water jet. The cooling water temperature is set at temperature (293 K) which is easy to obtain for practical use. Gravity (9.81 m/s^2) is considered in the model. The fuel (methane) and oxidizer (oxygen) are injected to the downhole combustion chamber through separate conduits.

$$CH_4 + 2O_2 \rightarrow CO_2 + 2H_2O$$

The stoichiometric relationship between carbon dioxide and water is 1:2. Therefore, the volume fraction of carbon dioxide in the generated hydrothermal jet is initially set as 30%. Turbulent flow calculation is carried out by using Realizable $k - \varepsilon$ model, which is widely used at present

[7, 8, 12]. The viscous heating and energy model solved by FLUENT are also chosen. The semi-implicit method for pressure-linked equations (SIMPLE) algorithm with multi-grid solver is used to couple pressure and velocities. Under-relaxation factors are set as default values. The convergence criterion based on residuals is set as 1×10^{-4} for each equation. The initial interval size of the mesh is 0.6. Other grids are checked for grid independence and produce similar results.

3. Results and discussion

3.1 Bottomhole thermal-physical property

The thermal-physical properties of the water and carbon dioxide are examined in this paper to indicate the accuracy of the simulation results. **Fig. 4** shows the distributions of water density, specific heat, thermal conductivity and viscosity. It can be observed that the maximum density lies in the region of cooling water. The highest value of the specific heat is at the boundary of annular hydrothermal jet and cooling water due to going through the PCP. In addition, the water thermal conductivity and viscosity also exhibit simulation results, which correspond with the real properties of water. For the carbon dioxide, **Fig. 5** shows the distributions of properties. The carbon dioxide is mainly distributed relatively far from the cooling water inlets. The thermal-physical properties of carbon dioxide keep almost the same in the entire wellbore. The density of carbon dioxide can be as low as 223 kg/m^3. Besides, different from water, the thermal conductivity and viscosity of carbon dioxide increase as the rise of temperature, which are also reasonable within suitable ranges. Therefore, it can be assumed that the simulation results in this paper are reasonable for engineering calculations.

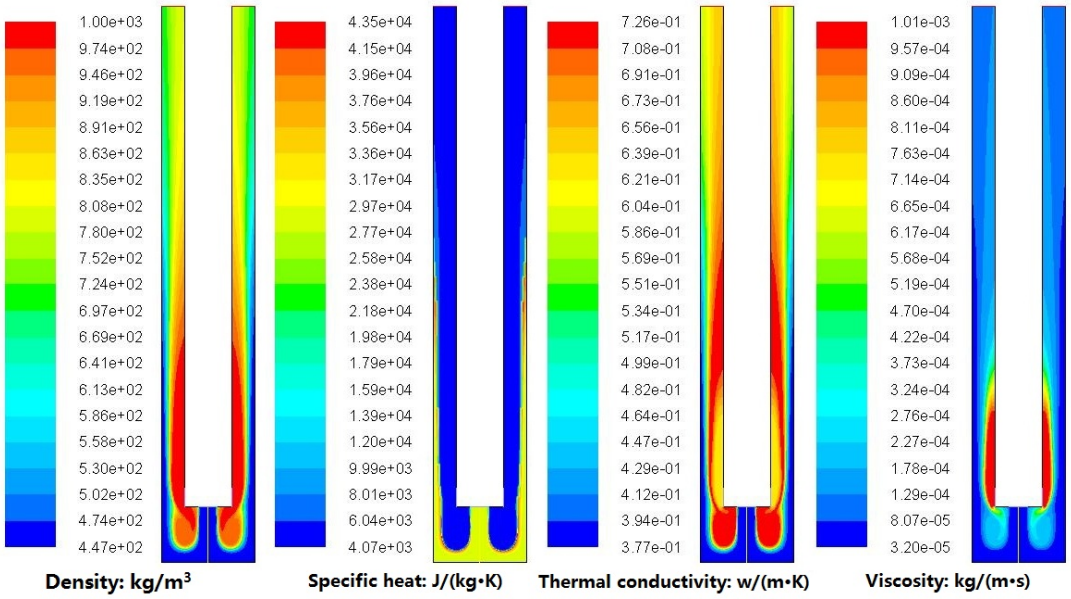

Figure 4: Contours of properties of water in the downhole flow field

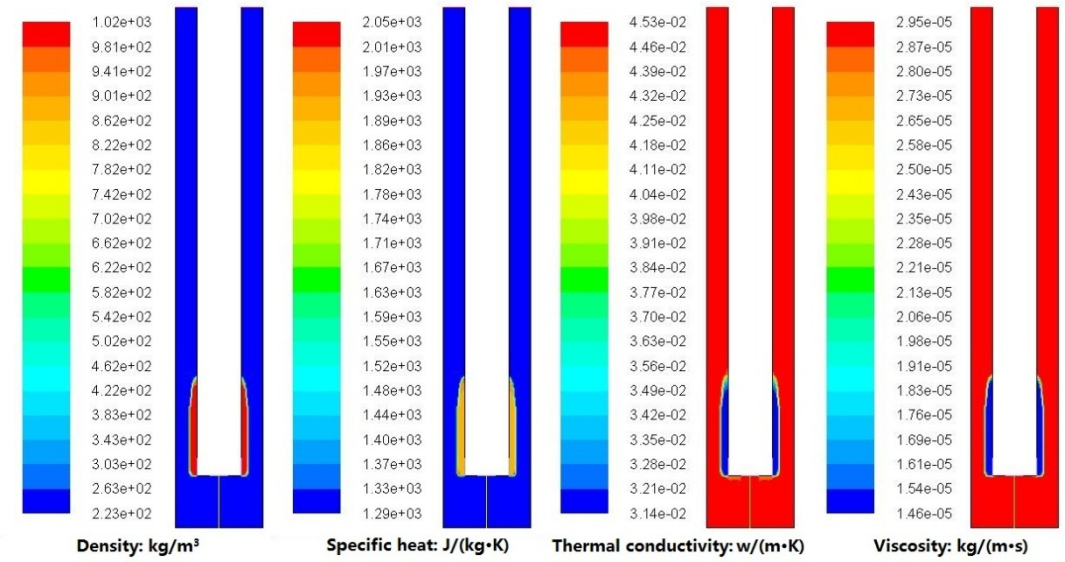

Figure 5: Contours of properties of carbon dioxide in the downhole flow field

3.2 Effects of jet velocity

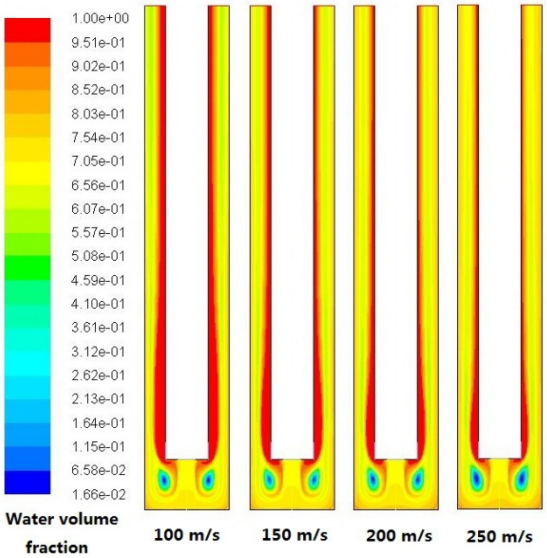

Figure 6: Contours of water volume fraction at different jet velocities

The hydrothermal jet velocity can be adjusted during drilling, such as changing the geometry of the nozzle. The influence of the jet velocity on downhole flow field is investigated. **Fig. 6** and **Fig. 7** show the contours of water and carbon dioxide volume fraction at the jet velocities of 100 m/s, 150 m/s, 200 m/s and 250 m/s. The initial volume fractions of water and carbon dioxide are 70% and 30%, respectively. Through comparison, it can be observed that the water occupies the most downhole space. There are two vertexes distributed at the two sides of the central hydrothermal jet, where the water volume fraction is relatively low of approximately 2 %. However, the volume fraction of carbon dioxide in these two vertexes is relatively high, even higher the initial fraction. This means that a portion of carbon dioxide circulates in the bottomhole space. In addition, the increase of jet velocity has no obvious effect on the overall

distributions of water and carbon dioxide. Nevertheless, with the increasing quantity of hydrothermal jet, the area of cooling water in the annulus is compressed to be smaller.

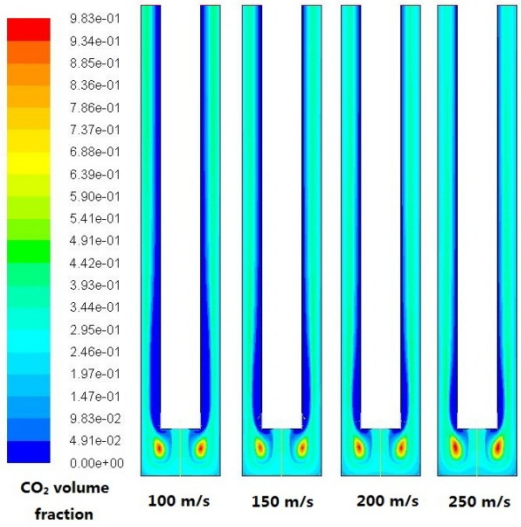

Figure 7: Contours of carbon dioxide volume fraction at different jet velocities

The downhole temperature of water is adopted to represent the wellbore temperature in this paper since the water is dominant in the hydrothermal jet drilling. As shown in **Fig. 8**, it can be seen that bottomhole temperatures keep almost the same at different jet velocities. The high temperature jet impinges on the bottom rock, and then backs upwards from the annulus. However, the two vertexes described above show relatively low temperature. Besides, as the jet velocity increases, the affected area of cooling water becomes smaller because of less heat transfer time. The overall annular temperature goes up. The velocity of the hydrothermal jet needs to be controlled well during drilling in the field to prevent too high temperature in the annulus.

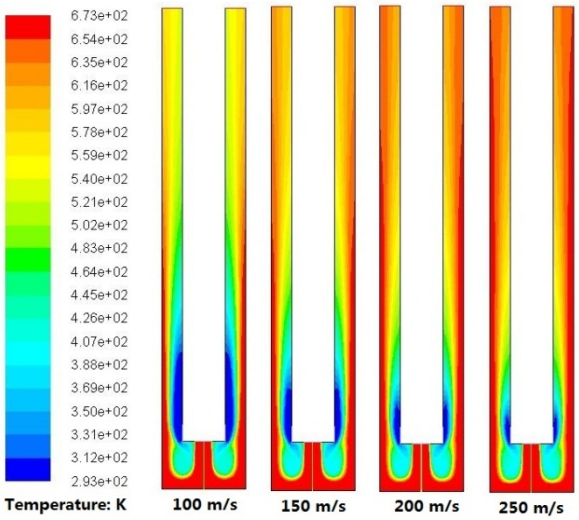

Figure 8: Contours of downhole temperature at different jet velocities

Besides the effect of high temperature, the impact pressure on the bottom rock is another important element for the realization of hydrothermal jet drilling. **Fig. 9** shows the bottomhole distributions of pressure. The pressure is the actual value impinging on the bottom rock besides the initial ambient rock pressure. There are fluctuations of pressure in the well bottom at each jet velocity. The well bottom center pressure is relatively high due to the direction impact. Besides, the pressure at the boundary of the well bottom is also relatively high because of the back force of the annular return fluid. At 100 m/s, the well bottom center pressure is approximately 2 MPa. As the increase of jet velocity, the bottomhole pressure becomes higher. The maximum value can be up to 8.5 MPa in this paper.

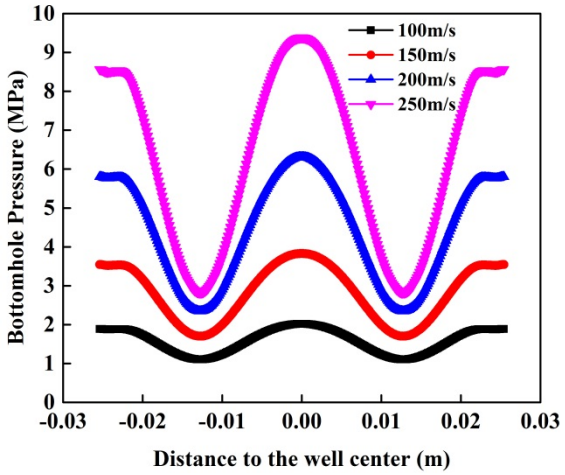

Figure 9: Distributions of bottomhole pressure at different jet velocities

3.3 Effects of jet temperature

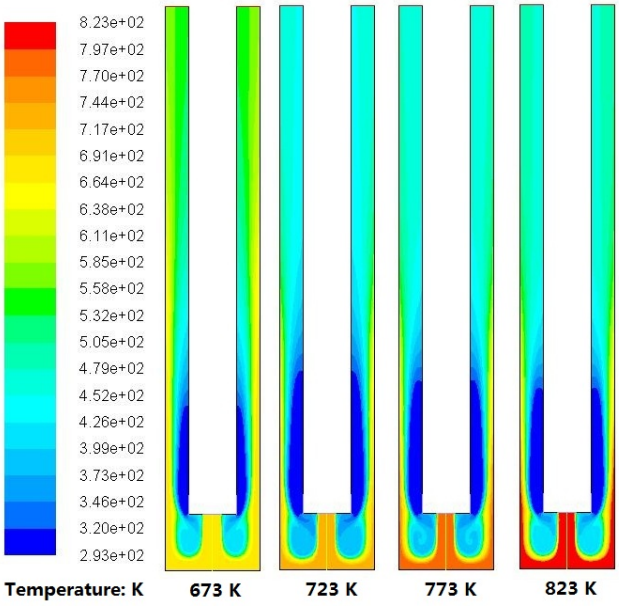

Figure 10: Contours of downhole temperature at different jet temperatures

Fig. 10 shows the contours of downhole temperature at different jet temperatures. It can be seen that the overall temperature distributions are similar. In the bottomhole space, especially on the well bottom, the temperature nearly keeps the same as the initial hydrothermal jet temperature. The region of the lowest temperature keeps nearly the same despite the variation of jet temperature. However, the annular temperature decreases from 673 K to 723 K, unexpectedly under the conditions of this paper. This may indicate that although the jet temperature becomes higher, the annular temperature may be able to be cooled effectively due to the complicated heat transfer between the hydrothermal jet and cooling water. However, this phenomenon still has to be validated by similar experiments. In **Fig. 11**, the bottom pressure is relatively high at 673 K mainly due to the relatively high density. When the jet temperature keeps rising, the pressure keeps almost the same and only decreases slightly.

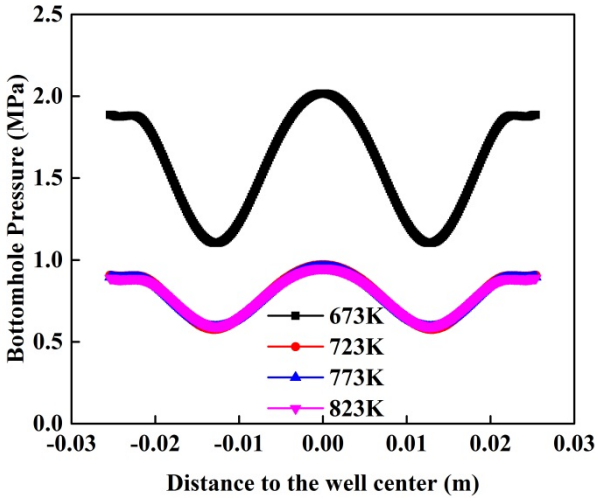

Figure 11: Distributions of bottomhole pressure at different jet temperatures

3.4 Effects of cooling water velocity

In the real application of hydrothermal jet drilling, the cooling water velocity can be adjusted to control the downhole temperature. **Fig. 12** shows the distributions of downhole temperature at different cooling water velocities. As the increase of cooling water velocity, the annulus can be cooled effectively and the low temperature region becomes larger. However, the temperature in the two vertexes becomes higher. The effect of the cooling water mainly acts on the annulus. **Fig. 13** displays the distributions of water volume fraction. The addition of cooling water makes the water volume fraction higher in the annulus. The area of two vertexes with low water volume fraction becomes larger.

With respect to the bottomhole pressure, as shown in **Fig. 14**, under the conditions of this paper the pressure increases as the rise of cooling water velocity. However, in this paper, the inlet boundary is set as constant velocity. In the downhole drilling condition, the flow direction of the annular return fluid is perpendicular to the cooling water, which makes the flow back of the bottomhole hydrothermal jet more difficult as the increase of cooling water velocity. To keep the inlet hydrothermal jet velocity constant, the injection pressure has to be increased to make the pressure drop the same. Therefore, the increase of bottomhole pressure may not be directly caused by the cooling water velocity, but more related to the set of simulation boundary conditions.

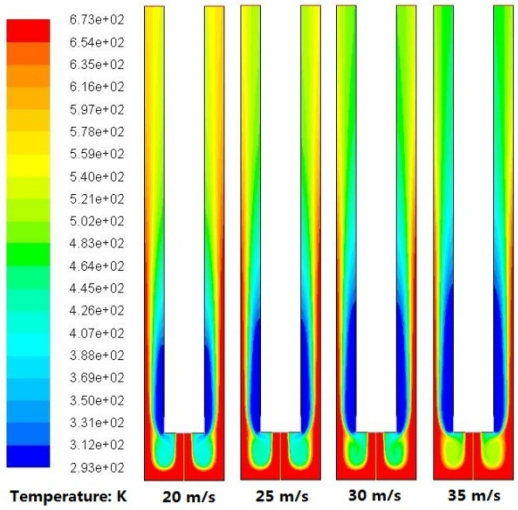

Figure 12: Distributions of downhole temperature at different cooling water velocities

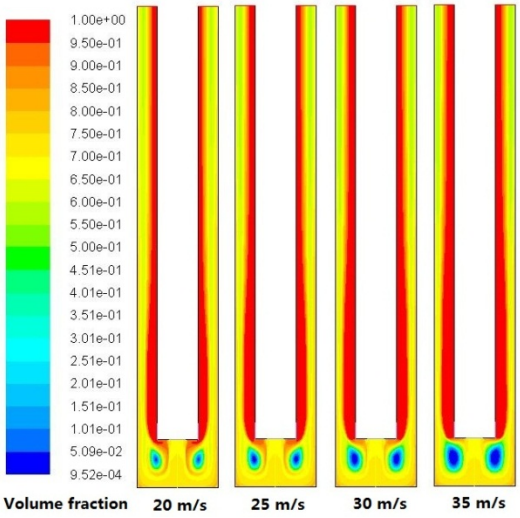

Figure 13: Distributions of water volume fraction at different cooling water velocities

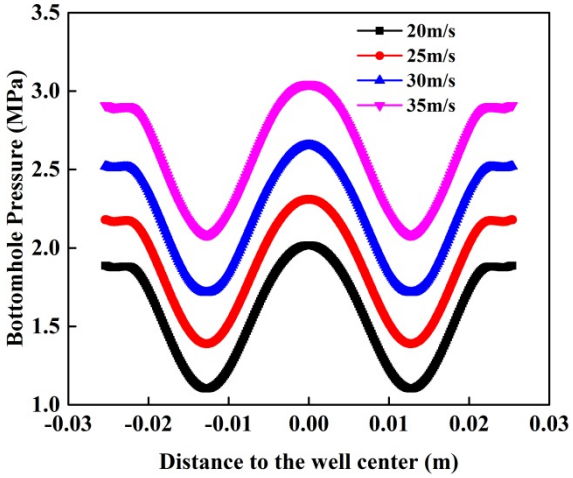

Figure 14: Distributions of bottomhole pressure at different cooling water velocities

3.5 Effects of carbon dioxide volume fraction

The above simulation of water and carbon dioxide volume fraction are based on the stoichiometric relationship. In hydrothermal jet drilling, additional water can be injected to the reactor to enhance the generation of hydrothermal jet. Consequently, the water volume fraction can be increased or carbon dioxide fraction can be decreased in the final generated jet.

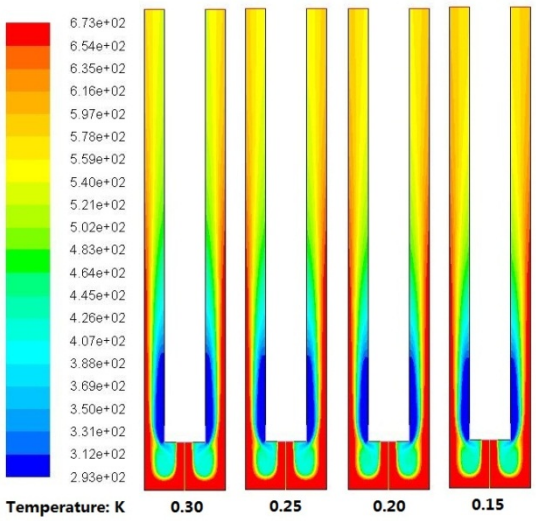

Figure 15: Distributions of downhole temperature at different carbon dioxide volume fractions

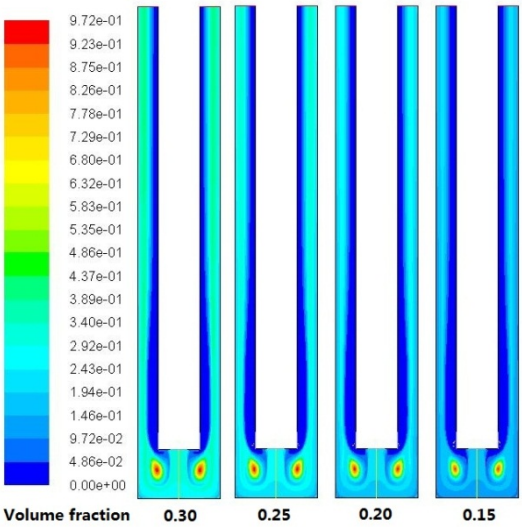

Figure 16: Distributions of carbon dioxide volume fraction at different carbon dioxide fractions

Fig. 15 shows the downhole temperature at different carbon dioxide volume fractions. The increase of water amount has no influence on the entire temperature distribution. Instead, it certainly affects the volume fraction of carbon dioxide as shown in **Fig. 16**. In both annulus and two vertexes, the volume fraction of carbon dioxide decreases. As for the bottomhole pressure, under the condition of constant jet velocity, the final pressure impinging on the bottom rock is most related to the jet density. The addition of the water volume fraction changes the components or density of the hydrothermal jet. Using the simulation models in this paper, as

shown in **Fig. 17**, the bottomhole pressure keeps nearly the same because the densities of carbon dioxide and water in supercritical state are close to one another. To be more specific, the pressure rises slightly with the increase of water volume fraction.

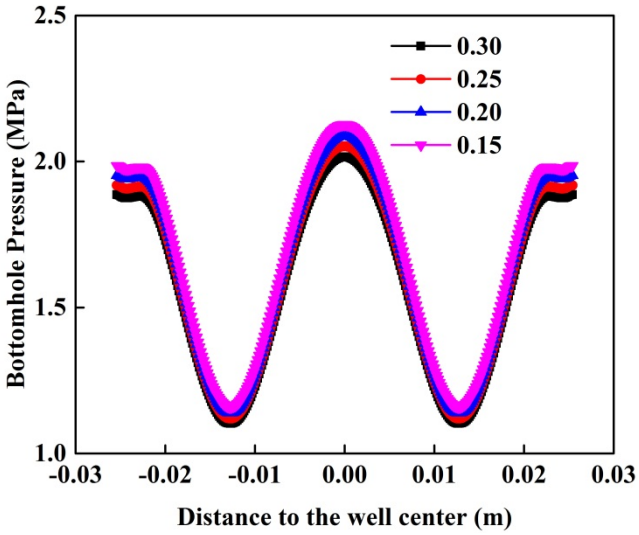

Figure 17: Distributions of bottomhole pressure at different carbon dioxide volume fractions

4. Conclusions

The simulation results in this paper are reasonable for engineering calculations by analyzing the distributions of simulated thermal-physical properties. There are two vertexes distributed at the two sides of the central hydrothermal jet, where the water volume fraction is relatively low. The increase of jet velocity has no obvious effect on the overall distributions of water and carbon dioxide. However, the velocity of the hydrothermal jet needs to be controlled well during drilling in the field to prevent too high temperature in the annulus. As the increase of jet velocity, the bottomhole pressure becomes higher. The maximum value can be up to 8.5 MPa in this paper.

Although the jet temperature becomes higher, the annular temperature may be able to be cooled effectively due to the complicated heat transfer between the hydrothermal jet and cooling water. However, this phenomenon still has to be validated by similar experiments. The jet temperature may also reduce the jet pressure. The cooling water velocity can lower the annular temperature effectively, but the effect on the pressure has to be further studied through experiments. The increase of water fraction may raise the jet pressure slightly.

Acknowledgments

The authors would like to acknowledge the National Key Research and Development Program of China (2016YFE0124600), Program of Introducing Talents of Discipline to Chinese Universities (111 Plan) (B17045) and National Natural Science Foundation of China (51504272, U1562212, 51521063). Besides, support from Special Fund of Ministry of Education for Authors of Outstanding Doctoral Dissertations (201352) and China National Petroleum Corporation Innovation Fund (2015D-5006-0308) and New Technique and Method Fund (2016A-3902) are appreciated.

REFERENCES

[1] X. Song, Z. Lv, G. Li, et al. Numerical analysis of characteristics of multi-orifice nozzle hydrothermal jet impact flow field and heat transfer[J], Journal of Natural Gas Science and Engineering, 2016, 35, 79-88.

[2] X. Song, Z. Lv, G. Li, et al. Numerical analysis on the impact of the flow field of hydrothermal jet drilling for geothermal wells in a confined cooling environment[J]. Geothermics, 2017, 39–49.

[3] Heard, H., 1980. Thermal expansion and inferred permeability of climax quartz monzonite to 300℃ and 27.6MPa. Int J Rock Mech Min Sci&GeomechAbstr. 1980, 289-296.

[4] Li, J., Guo, B., Yang, S., Liu, G., 2014. The complexity of thermal effect on rock failure in gas-drilling shale-gas wells. Journal of Natural Gas Science and Engineering. 2014, 255-259.

[5] Maurer, W.C, Heilhecker, J.K, 1969. Hydraulic Jet Drilling. Paper of the Drilling and Rock Mechanics Symposium.

[6] Pols, A.C., 1977. High-pressure jet-drilling experiments in some hard rocks. J. Press. Vessel Technol. 99 (2), 353-361.

[7] Martin, J., Tobias, R., Philipp, R., 2013. Simulation of the thermal field of submerged supercritical water jets at near-critical pressures. The Journal of Supercritical Fluids. 2013, 128-137.

[8] Martin J., Tobias R., Philipp, R., 2013. Numerical analysis of penetration lengths in submerged supercritical water jets. The Journal of Supercritical Fluids. 2013, 82, 213-220.

[9] Wagner W. The IAPWS Formulation 1995 for the Thermodynamic Properties of Ordinary Water Substance for General and Scientific Use[J]. Journal of Physical & Chemical Reference Data, 2002, 31(2), 387-535.

[10] Peng, Y., Ma, C., 2005. Technical Application Manual of Supercritical Fluid. 2005, 417-437.

[11] D. Peng, D.B. Robinson, A New Two-Constant Equation of State, 15 (1976), 59–64.

[12] Tobias R. et al., Heat transfer phenomena of supercritical water jets in hydrothermal spallation drilling. 2013.